The Institute of Space and Astronautical Science
Report No. 607, September 1983

Gas-Particle Mixture Flows in a Spinning Solid Rocket Motor

By

Masaya YAMAMOTO and Hakuro OGUCHI

(August 27, 1983)

Summary: Main aim of this studiy is to clarify the spin stabilization effect on the flow field. Internal flow field of the solid rocket motor is numerically analyzed by the time-dependent finite difference method in combination with the boundary-fitted curvilinear coordinate technique. Computation was carried out about flow through the nozzle with cigarette-burn type chamber and also with spherical chamber. The thrust performance and the behavior of the particle impingement upon nozzle wall were analyzed. As the results, the followings are shown,

(1) The thrust loss caused by two-phase flow is less for the nozzle with cigarette-burn type chamber, than for the nozzle with spherical chamber.
(2) As to the nozzle with cigarette-burn type chamber, the thrust loss of 2 to 3 percent occurs under the 2 r.p.s. spin stabilization. In no-spin case, particle impingement is not observed over a whole nozzle wall, while in the case of spin stabilization it is observed on the nozzle wall near the exit.
(3) As to the nozzle with spherical chamber, there is no appreciable effect of the spin stabilization.

I. INTRODUCTION

The solid propellants are generally mixed with metalic powder for the purpose of achieving higher burning temperature, and thus the chamber and nozzle flow contain many oxidized metal particles. The flow behaviors differentiate from one-phase flow. So far, the evaluation of thrust performance and the prediction of particle impingement upon nozzle wall have been done by many investigators [*1–4*]. Further elaborate analysis of these two problems is still very important for design of a solid rocket motor from the view point of motor re-usage. The difficulty of these analysis arises from two-phase nature, from sub- to supersonic regine.

The aim of this study is to provide a precise evaluation of the thrust performance and a prediction of the particle impingement upon nozzle wall under the spin stabilization. The spin stabilization causes the change of flow field; an additional swirling flow appaers. The works, so far made, do not take into account the spin effect. This study attempts to analyze numerically by the transient (time-dependent) technique [*5–6*] whole flow field of the solid rocket motor, ranging from the chamber to the nozzle exit, taking into account the spin effect.

II. Governing Equations

The equations governing the axisymmetric flow of the gas-particle mixture are derived from the following assumptions,

(1) The gas is an inviscid, perfect gas having no interaction with particles.
(2) The gas and particles have constant heat capacities.
(3) The gas and particles do not undergo phase changes.
(4) The internal temperature of particles is uniform.
(5) The volume occupied by the particles is negligibly small.
(6) There is no interaction between particles.
(7) The Brownian motion of particles is negligible.
(8) The size and shape of all particles are uniform.
(9) The viscous drag of particles is determined by an experimental relation [7] or the Stokes' law.
(10) The heat transfer contains the radiative heat transfer.

When, based on these assumptions, the quantities are normalized by the gas-phase stagnation state, sound speed and throat radius, the following equations govern the flow field of gas-particle mixture, continuity equation for gas-phase,

$$\frac{\partial \rho}{\partial t}+u\frac{\partial \rho}{\partial x}+v\frac{\partial \rho}{\partial r}+\rho\left(\frac{\partial u}{\partial x}+\frac{\partial v}{\partial r}\right)+\frac{\rho v}{r}=0, \tag{2-1}$$

axial, radial and circumferential momentum equations for gas-phase,

$$\frac{\partial u}{\partial t}+u\frac{\partial u}{\partial x}+v\frac{\partial u}{\partial r}+\frac{1}{\rho\gamma}\frac{\partial p}{\partial x}+Af\mu(u-u_p)\frac{\rho_p}{\rho}=0, \tag{2-2}$$

$$\frac{\partial v}{\partial t}+u\frac{\partial v}{\partial x}+v\frac{\partial v}{\partial r}+\frac{1}{\rho\gamma}\frac{\partial p}{\partial r}-\frac{w^2}{r}+Af\mu(v-v_p)\frac{\rho_p}{\rho}=0, \tag{2-3}$$

$$\frac{\partial w}{\partial t}+u\frac{\partial w}{\partial x}+v\frac{\partial w}{\partial r}+\frac{vw}{r}+Af\mu(w-w_p)\frac{\rho_p}{\rho}=0, \tag{2-4}$$

energy equation for gas-phase,

$$\begin{aligned}&\frac{\partial}{\partial t}\left\{\rho\left(\frac{1}{2}q^2+e\right)\right\}+u\left[\frac{\partial}{\partial x}\left\{\rho\left(\frac{1}{2}q^2+e\right)\right\}+\frac{1}{\gamma}\frac{\partial p}{\partial x}\right]\\&\quad+v\left[\frac{\partial}{\partial r}\left\{\rho\left(\frac{1}{2}q^2+e\right)\right\}+\frac{1}{\gamma}\frac{\partial p}{\partial r}\right]+\left\{\rho\left(\frac{1}{2}q^2+e\right)+\frac{p}{\gamma}\right\}\frac{v}{r}\\&\quad+\left\{\rho\left(\frac{1}{2}q^2+e\right)+\frac{p}{\gamma}\right\}\left(\frac{\partial u}{\partial x}+\frac{\partial v}{\partial r}\right)\\&\quad+A\rho_p[f\mu\{(u-u_p)u_p+(v-v_p)v_p+(w-w_p)w_p\}\\&\quad+B(T-T_p)+C(\varepsilon T^4-\varepsilon_p T_p^4)]=0,\end{aligned} \tag{2-5}$$

continuity equation for particle-phase,

$$\frac{\partial \rho_p}{\partial t}+u_p\frac{\partial \rho_p}{\partial x}+v_p\frac{\partial \rho_p}{\partial r}+\rho_p\left(\frac{\partial u_p}{\partial x}+\frac{\partial v_p}{\partial r}\right)+\frac{\rho_p v_p}{r}=0, \tag{2-6}$$

axial, radial and circumferential momentum equations for particle-phase,

$$\frac{\partial u_p}{\partial t}+u_p\frac{\partial u_p}{\partial x}+v_p\frac{\partial u_p}{\partial r}-Af\mu(u-u_p)=0, \tag{2-7}$$

$$\frac{\partial v_p}{\partial t}+u_p\frac{\partial v_p}{\partial x}+v_p\frac{\partial v_p}{\partial r}-\frac{w_p^2}{r}-Af\mu(v-v_p)=0, \tag{2-8}$$

$$\frac{\partial w_p}{\partial t}+u_p\frac{\partial w_p}{\partial x}+v_p\frac{\partial w_p}{\partial r}+\frac{v_p w_p}{r}-Af\mu(w-w_p)=0, \tag{2-9}$$

energy equation for particle-phase,

$$\begin{aligned}&\frac{\partial}{\partial t}\left\{\rho_p\left(\frac{1}{2}q_p^2+e_p\right)\right\}+u_p\frac{\partial}{\partial x}\left\{\rho_p\left(\frac{1}{2}q_p^2+e_p\right)\right\}+v_p\frac{\partial}{\partial r}\left\{\rho_p\left(\frac{1}{2}q_p^2+e_p\right)\right\}\\&+\rho_p\left(\frac{1}{2}q_p^2+e_p\right)\frac{v_p}{r}+\rho_p\left(\frac{1}{2}q_p^2+e_p\right)\left(\frac{\partial u_p}{\partial x}+\frac{\partial v_p}{\partial r}\right)\\&-A\rho_p[f\mu\{(u-u_p)u_p+(v-v_p)v_p+(w-w_p)w_p\}\\&+B(T-T_p)+C(\varepsilon T^4-\varepsilon_p T_p^4)]=0,\end{aligned} \tag{2-10}$$

where the subscript p indicates particle-phase. In the energy equations,

$$q^2=u^2+v^2+w^2, \tag{2-11}$$

$$q_p^2=u_p^2+v_p^2+w_p^2, \tag{2-12}$$

$$e=T/\gamma/(\gamma-1), \tag{2-13}$$

$$e_p=T_p cT_0/a_0^2. \tag{2-14}$$

In the friction term,

$$A=\frac{9l_0\mu_0}{2r_p^2Cm_p a_0}, \tag{2-15}$$

where

$$a_0=\sqrt{\gamma RT_0}. \tag{2-16}$$

In the heat transfer term,

$$B=\frac{2Nu}{3Pr(\gamma-1)}, \tag{2-17}$$

where

$$Nu=0.664Pr^{0.3}Re_p^{0.5}, \tag{2-18}$$

$$Pr=0.74\sim0.78, \tag{2-19}$$

with

$$Re_p = \frac{\rho_0 r_p a_0}{\mu_0} . \tag{2-20}$$

In the radiative heat transfer term,

$$C = \frac{2 r_p \sigma T_0^3}{3\mu_0 Cp(\gamma - 1)}, \tag{2-21}$$

The parameter f of the drag lag is for Stokes' law,

$$f = 1, \tag{2-22}$$

for experimental formula,

$$f = \frac{(1 + 0.15 Re_p^{0.678})\{1 + \exp(-0.427/M^{4.63} - 3.0/Re_p^{0.88})\}}{[1 + M\{3.82 + 1.28\exp(-1.25 Re_p/M)\}/Re_p]} . \tag{2-23}$$

The gas viscosity is the function of temperature and computed using the Southerland's formula:

$$\mu = \left(\frac{1 + ss}{T + ss}\right) T^{1.5}, \tag{2-24}$$

where

$$ss = 111/T_0. \tag{2-25}$$

III. Numerical Treatments

In the transonic region of gas-particle mixture flow, the mixed-type (elliptic and hyperbolic) governing equations cause some difficulty for the analytical treatment. In the numerical treatments, the transient technique can enable us to avoid its difficulty. In combining with the boundary-fitted curvilinear coordinate technique [8], it can be applied to analyze the nozzle flow of arbitrary configuration.

3.1 *Boundary-fitted curvilinear coodinate technique*

In order to transform an arbitrary nozzle shape in physical plane into a rectangular grid in computational plane, the solutions of two elliptical partial differential equations are used. Using Poisson's equations as the generating elliptic system,

$$\xi_{xx} + \xi_{yy} = P(\xi, \eta), \tag{3-1}$$

$$\eta_{xx} + \eta_{yy} = Q(\xi, \eta). \tag{3-2}$$

Now, in order to carry out numerical computation in the rectangular transformed plane, the dependent and independent variables must be changed,

$$\alpha x_{\xi\xi} - 2\beta x_{\xi\eta} + \gamma x_{\eta\eta} + J^2(P x_\xi + Q x_\eta) = 0, \tag{3-3}$$

$$\alpha y_{\xi\xi} - 2\beta y_{\xi\eta} + \gamma y_{\eta\eta} + J^2(P y_\xi + Q y_\eta) = 0, \tag{3-4}$$

where

$$\alpha = x_\eta^2 + y_\eta^2, \tag{3-5}$$

$$\beta = x_\xi x_\eta + y_\xi y_\eta, \tag{3-6}$$

$$\gamma = x_\xi^2 + y_\xi^2, \tag{3-7}$$

$$J = x_\xi y_\eta - x_\eta y_\xi. \tag{3-8}$$

In the transformed plane, the derivatives are transformed into the followings,

$$f_x = (y_\eta f_\xi - y_\xi f_\eta)/J, \tag{3-9}$$

$$f_y = (-x_\eta f_\xi + x_\xi f_\eta)/J. \tag{3-10}$$

Using the succesive over relaxation method, coordinates, derivatives and Jacobian which are necessary for transformation are computed and stored in file for later use.

3.2 *The hopscotch finite difference method*

For the solution, the hopscotch finite difference method is adopted. The hospcotch finite difference method is a two-step explict procedure, presented by Gourlay [*6*]. Let us consider, for example, the equation

$$\vec{u}_t = F(\vec{u}_x, \vec{u}_y). \tag{3-11}$$

At first sweep, with forward time and centered space differencing, $\vec{u}_{i,j}^{n+1}$, is computed at each time step at the nodes, for which $i+j+n$ is even (Fig. 1); namely,

$$\vec{u}_{i,j}^{n+1} = \vec{u}_{i,j}^{n} - \Delta t * F(\vec{u}_x^n, \vec{u}_y^n). \tag{3-12}$$

In this sweep, the computation is fully explicit. Then second sweep at the nodes, for which $i+j+n$ is odd, is

$$\vec{u}_{i,j}^{n+1} = \vec{u}_{i,j}^{n} - \Delta t * F(\vec{u}_x^{n+1}, \vec{u}_y^{n+1}). \tag{3-13}$$

This sweep seems to be formally implicit. However, the spatial derivatives involved

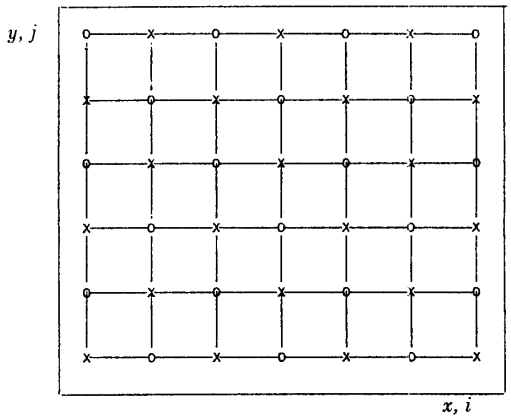

Fig. 1. Hopscotch Grid.
1st sweep; $i+j+n$ even 0
2nd sweep; $i+j+n$ odd ×

in F are computed from the $\vec{u}_{i,j}^{n+1}$ already evaluated at first sweep. Therefore, this method is fully explicit method.

As is mentioned above, it is noted that at second sweep the n-time step values at the nodes, for which $i+j+n$ is even, are not needed for computation. Consequently, the computer-storage is saved to the extent much less than that of ordinary explicit finite difference methods, e.g. MacCormack finite difference method. This scheme is more favorable for the solution of the equations containing many dependent variables.

3.3 *Initial conditions*

For one-phase flow, the solutions of quasi-one-dimensional analysis were assumed as the initial conditions. For gas-particle mixture, the solution for one-phase flow analysis was taken as the initial conditions, assuming that particles are in perfect equilibrium with gas.

3.4 *Boundary conditions*

At the source boundary (burning surface) the fixed flow variables that satisfy with stagnation conditions are used. If, for a fixed motor-nozzle configuration, the stagnation condition of the flow is specified, the condition at the source boundary is evaluated from quasi-one-dimensional flow analysis. For two-phase flow, velocities and temperature lags are assumed zero at the source boundary. On the axis, axisymmetric condition is used. However, in this study, fluid is inviscid and slips on the wall, so tangency condition is employed.

Since the flow is supersonic at the exit, the *2nd*-order extrapolation from interior points is applied of the exit boundary.

In the transonic region, the instability was sometimes experienced at the initial stage of the computation. To avoid such an instability, a sort of damping factor (say second or forth order derivatives of the flow velocities) was introduced only at the initial stage. After the solution has been stabilized, these damping factors are removed. The solution thus obtained is regarded as the exact one for governing euqations.

IV. Results and Discussion

4.1. *Test of the numerical method*

For test of the numerical method, comparison with experimental data [*10*] about JPL nozzle flow (one-phase) was done in the frame of the grid shown in Fig. 2. The parameters and constants employed are summarized in Table 1. Mach number distributions in both experiment and computation are shown in Fig. 3. In case of such small radius-of-curvature throat, the computational results agree well with the experiment over the whole flow region except near the wall downstream from the throat. The diviation from the experiment near the wall downstream the throat is likely to result from the effect of viscosity, say boundary layer, which is not considered in this computation. The computational results indicate a same tendency with other computational result [*11*] obtained for the same JPL nozzle configuration.

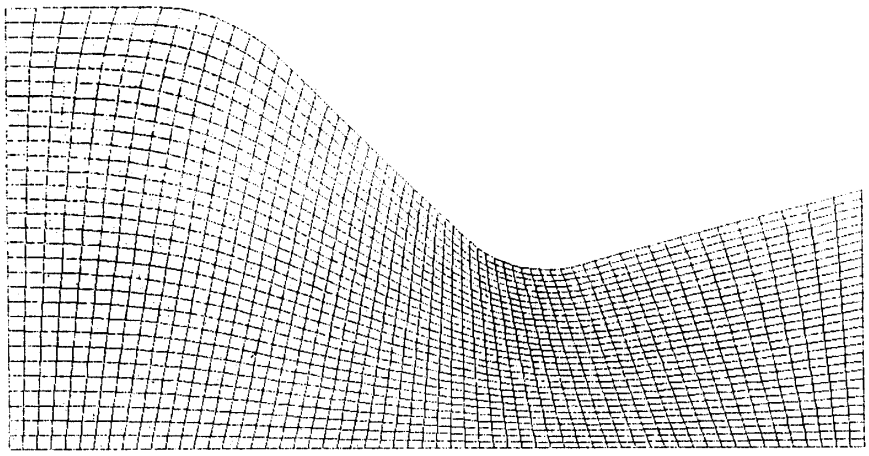

Fig. 2. Grid for JPL nozzle.

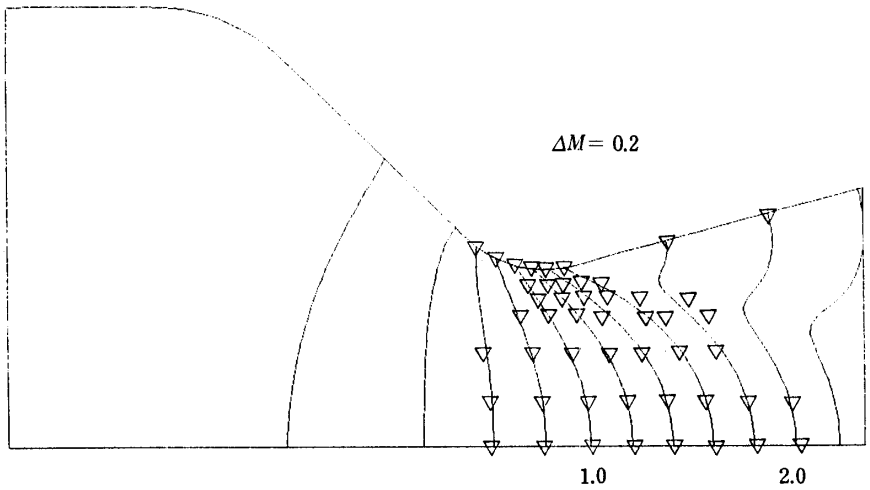

Fig. 3. Comparison of computational results with experimental data in the transonic region.
Symbols regprsent experimental data from Ref. 10.

Table 1 Parameters and constants

	JPL	Case 1	Case 2
Stagnation temperature (K)	555.56	3144.0	3144.0
Stagnation pressure (N/m^2)	1034.2×10^3	3920.0×10^3	3920.0×10^3
Gas specific heat ratio	1.0	1.2035	1.2035
Gas specific heat at constant pressure (J/kg/K)	1070.0	1686.0	1686.0
Particle heat capacity (J/kg/K)	1380.0	1340.0	1340.0
Mass fraction	0.3	0.302	0.302
Particle mass density (kg/m^3)	4004.62	3203.69	3203.69
Gas viscosity at stagnation (kg/m/sec)	2.68×10^{-5}	6.3×10^{-5}	6.3×10^{-5}
Gas emissivity	0.05	0.05	0.05
Particle emissivity	0.11	0.11	0.11
Throat radius (m)	1.59×10^{-2}	7.6×10^{-2}	7.6×10^{-2}
Prandtl number	0.74	0.7795	0.7795

From the fact as mentioned above this method is expected to be acceptable for the numerical analysis of the one-phase nozzle flow. In the same nozzle, two-phase flow analysis was carried out, and the outline of the two-phase flow was grasped.

Further numerical analyses were done for two nozzle configurations; Case 1 is of a nozzle with the gentle-radius-of-curvature throat (Fig. 4), and Case 2 is of a nozzle with spherical chamber, as used in an upper stage motor (Fig. 10). Especially, Case 2 was chosen as an attempt to solve the whole flow field of chamber and nozzle. In each case, analyses contain one-phase flow, and two-phase flow. In these cases, two-phase flow with spin effect is dealt with. Detail of the results is presented in the following sections.

4.2 *Case 1*

The computational grid is also shown in Fig. 4. The parameters and constants are summarized in Table 1.

a) one-phase flow

This nozzle has more gentle radius-of-curvature throat compared with JPL nozzle. The points of inflection appear on the lines of constant Mach number in supersonic region (Fig. 5). The points of inflection are caused by the unusual expansion characteristics originating from the change in wall curvature; these points lie on the characteristic line initiating from the junction of curved throat with straight divergent wall. The locus of these points of inflection must be apparent in an inviscid fluid. As can be seen from Fig. 5, however they are slightly smeared. In this analysis, an error inevitably involved in the computation of difference scheme plays a role of artificial viscosity, so the flow behaves viscous-like.

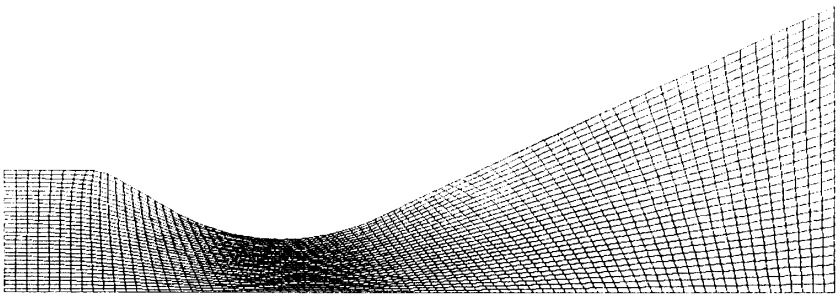

Fig. 4. Grid for the nozzle of Case 1.

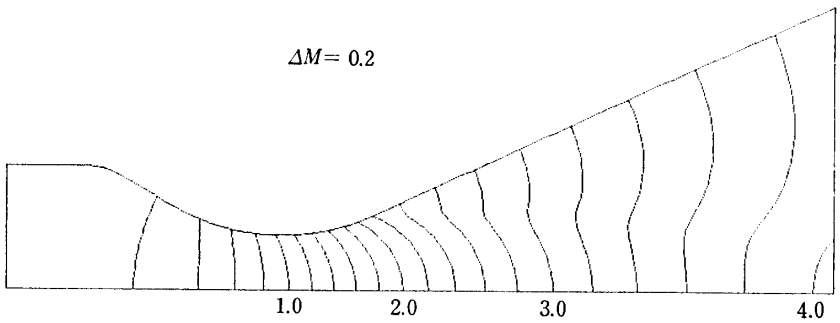

Fig. 5. Controus of Mach number in one-phase flow.

b) two-phase flow

Because of existence of particles, the flow field of gas-particle mixture is far different from one-phase flow. Physical variables of gas (pressure, temperature, density and velocities) indicate different distribution from one-phase flow. Mach number contours of two-phase flow are shown in Fig. 6 for particle radius 2 μm. The equi-Mach number lines have also the points of inflection, but they do not appear so apparently and inconspicuous compared with the case of one-phase flow.

The appearance of the shear layers near the wall is contrast to the one-phase flow. The particles are accelerated by interaction with gas only. The particles cannot follow the abrupt velocity change in radial direction near the throat. In the divergent region, therefore particles do not exist near the wall (Fig. 7). Conversely, gas is dragged by the particles, so that velocity of gas is less than that of one-phase flow at the same point. In the region, where many particles exist, the deceleration of gas is so large that the shear layer is build up.

The flow field does not relax; namely, velocity lags and temperature difference exist between gas and particles. Since the particles are accelerated by gas, naturally there exists a velocity lag between gas and particles in the region where gas is accelerated. The existence of temperature difference between gas and particles is also natural, because through acceleration the gas is cooled down while the particles are not so.

Similar nature of the flow field is obtained in the case of 4 μm particle radius. In the comparison with smaller particle radius case (2 μm), characteristics pertinent to

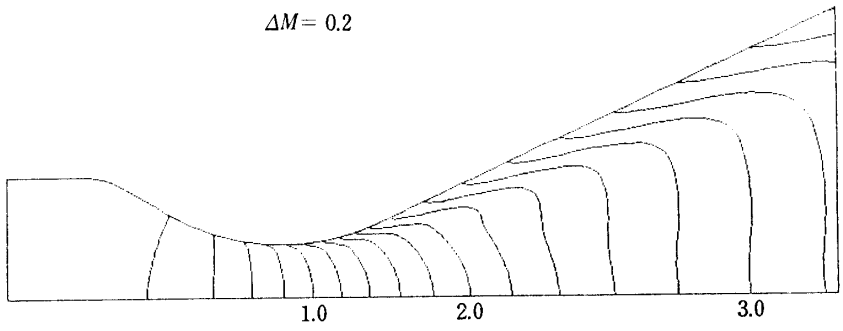

Fig. 6. Controus of Mach number in two-phase flow. Radius of particle is 2 μm.

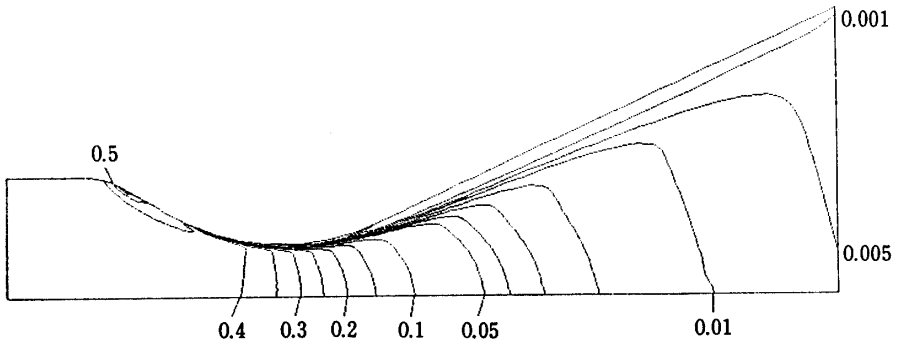

Fig. 7. Contours of particle density. Radius of particle is 2 μm.

the two-phase flow are much emphasized and particle-free zone is enlarged. Gas velocities are slower than those of previous case, deceleration rate depending on particle size.

Thrust performance is indicated in Table 2. As can be seen from this table, the thrust loss caused by two-phase flow is estimated about 8 percent in 2 μm case and 8.1 percent in 4 μm case.

c) spin effect

In order to simulate the effect of spin stabilization on the nozzle flow, the flow on the source boundary is assumed to be in solid rotation. Gas is also assumed inviscid, and thus the resulting flow becomes a swirling flow. Circumferential velocity profile

Table 2 Thrust performances

		ISP (sec)	Particle size (μm)
Case 1	One-phase flow	259.42	—
Case 1	Two-phase flow	238.83	2
Case 1	Two-phase flow under spin	231.47	2
Case 1	Two-phase flow	238.31	4
Case 1	Two-phase flow under spin	232.42	4
Case 2	One-phsae flow	264.12	—
Case 2	Two-phase flow	229.05	2
Case 2	Two-phase flow under spin	229.03	2

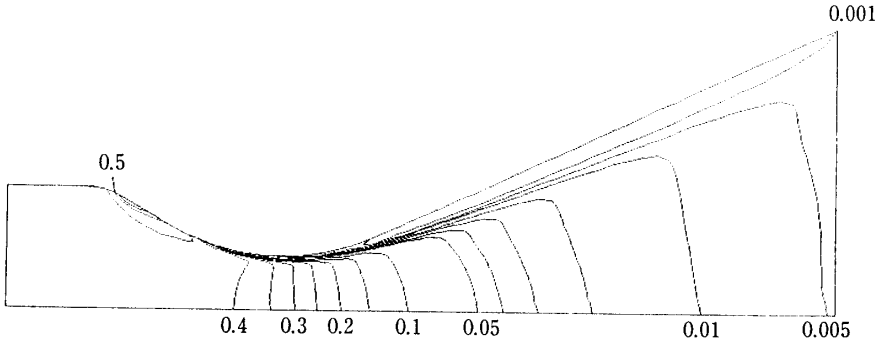

Fig. 8. Contours of particle density in Case 1. Radius of particle is 2 μm. Spin rate is 2 r.p.s..

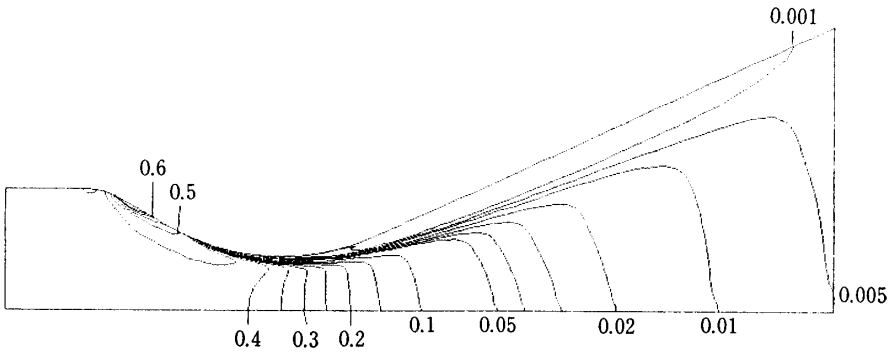

Fig. 9. Contours of particle density in Case 1. Radius of particle is 4 μm. Spin rate is 2 r.p.s..

was distributed, in a similar way to a solid rotation, from the source boundary to the exit. Then, both centrifugal force and Coriolis' force give influence on the flow field. In the divergent region, radial expansion of particles is much enhanced than that of no swirling flow. Therefore the particles tend to distribute towards outerside (Fig. 8). In the case of larger particle size, such tendency becomes more appreciable. This can be seen from Fig. 9. When the decelerated area of gas becomes larger, the thrust performance declines. Thrust performances are summarized in Table 2. The spin effect on the thrust performance loss is 2 to 3 percent. Particle impingement on the wall appears near the exit in both cases of 2 and 4 μm particles. This is clearly caused by the spin stabilization effect. Evidently, the range of the impingement depends on the particle size.

4.3. *Case 2*

In this case, the flow field of the nozzle with spherical chamber is treated. The characteristics of the flow field are similar to those of previous case. However, the circumferential velocity distribution is different from that of Case 1, because of the different configuration of the source boundary. Constants and parameters are summarized in Table 1.

a) one-phase flow

The computational grid is shown in Fig. 10. Fluid issues not only from the axial direction but also from the radial direction. Therefore, the pattern of flow field is different from that of Case 1 in the subsonic region (Fig. 11). In this case the characteristic line, which initiates from the junction of the throat with the straight wall, also can be

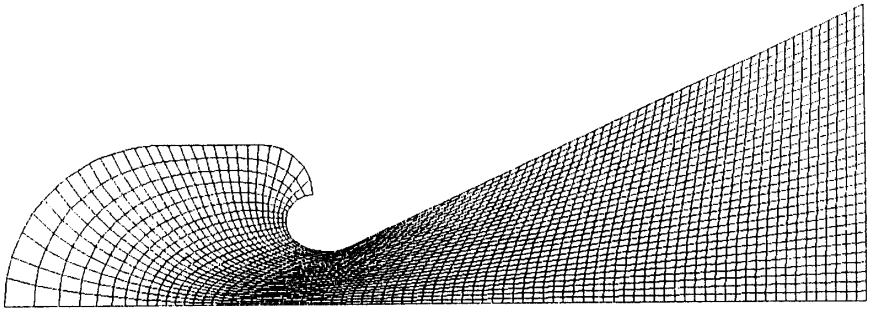

Fig. 10. Grid for the nozzle of Case 2.

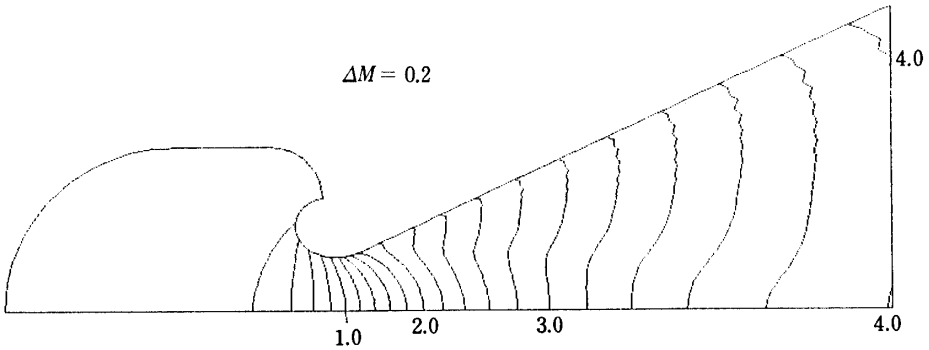

Fig. 11. Contours of Mach number in one-phase flow.

seen. But this line crosses the axis at upsteam than in Case 1, on account of small-radius-of-curvature throat. Other features of the flow field are similar to those of Case 1.

b) two-phase flow

The contours of Mach number and particle density are shown in Figs. 12–13. The thrust loss in two-phase flow is larger than that in Case 1 of the nozzle with the cigarette-burn type.

c) spin effect

The characteristics of the flow field are the same as Case 1 except the circumferential velocity profile. The rocket motor itself spins in solid rotation, but the fluid was not

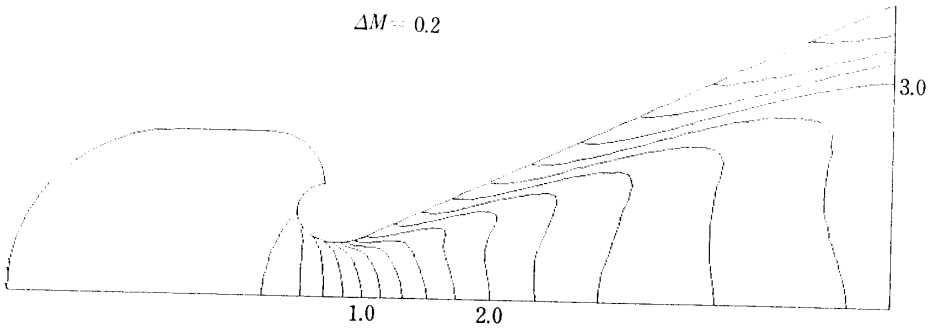

Fig. 12. Contours of Mach number in Case 2. Radius of particle is 2 μm.

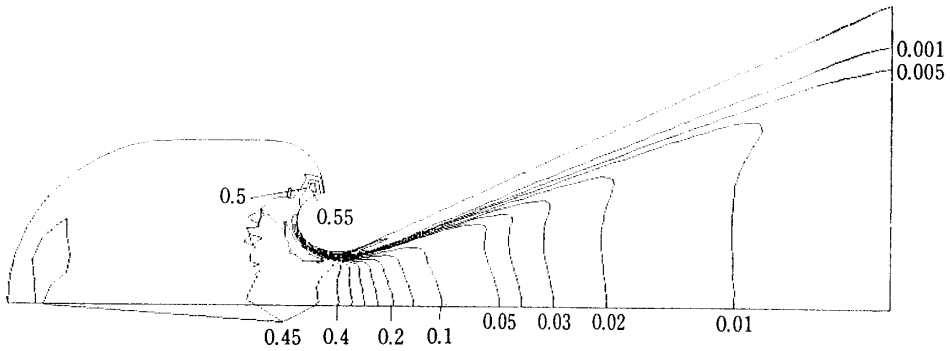

Fig. 13. Contours of particle density in Case 2. Radius of particle is 2 μm.

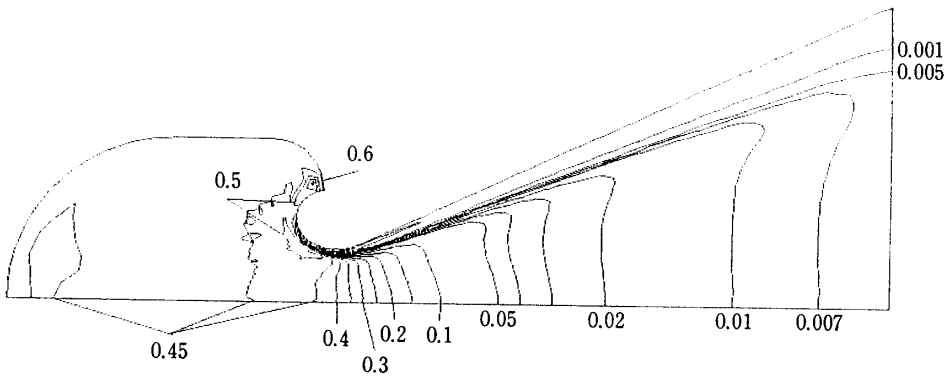

Fig. 14. Contours of particle density in Case 2 under the spin stabilization. Radius of particle is 2 μm. Spin rate is 2 r.p.s..

in the same spin over the region downstream from the transonic region; i.e. the fluid was not in solid rotation. There is only a weak effect of spin stabilization on the flow behavior, so that the thrust loss is negligible in this case (Table 2). This is mainly due to the slower circumferential velocity in the outer region far from the axis. Therefore, such a weak centrifugal force cannot bring particles toward the outer side (Fig. 14).

V. Concluding Remarks

The effect of the spin stabilization on the internal gas-particle mixture flow field of the solid rocket motor is studied numerically by the hopscotch finite difference method combined with the boundary-fitted curvilinear coordinate technique. The computation code used in this analysis can be used even in the computer system with small storage. The damping for the elimination of instability is only used during the initial stage of computation. The resulting solution may be regarded as an exact solution of governing equations, because the additional damping factors are removed after the initial stage of computation. The results agree well with the experimental data and the results of other numerical analyses for JPL nozzle.

In conclusion, the following results available for the design of a solid rocket motor have been obtained, especially concerning the effects of the spin stabilization and also the chamber configuration.

(1) The thrust loss caused by two-phase flow is less for the nozzle with cigarette-burn type chamber, than for the nozzle with spherical chamber.

(2) As to the nozzle with cigarette-burn type chamber, the thrust loss of 2 to 3 percent occurs under the 2 r.p.s. spin stabilization. In no-spin case, particle impingement is not observed over a whole nozzle wall, while in the case of spin stabilization it is observed on the nozzle wall near the exit.

(3) As to the nozzle with spherical chamber, there is no appreciable effect of the spin stabilization.

For further applications, this code can be employed for the analysis on the flow field of swirling combustion with large swirling ratio.

Nomenclature

a_0 sonic speed at stagnation state
A dimensionless friction term defined in Eq. (2–15)
B dimensionless heat transfer term defined in Eq. (2–17)
C dimensionless radiative heat transfer term defined in Eq. (2–20); particle specific heat
Cm_p particle mass density
Cp gas specific heat at constant pressure
e dimensionless gas internal energy per unit mass defined in Eq. (2–13)
e_p dimensionless particle internal energy per unit mass defined in Eq. (2–14)
f parameter of drag
F vector defined in Eq. (3–11)

J Jacobian of transformation
l_0 refernce length; throat radius
M gas phase Mach number
Nu particle Nusselt number
p dimensionless pressure
P controll function of grid
Pr gas-phase Prantle number
q^2 dimensionless gas momentum energy per unit mass defined in Eq. (2–11)
q_p^2 dimensionless particle momentum energy per unit mass defined in Eq. (2–12)
Q controll function of grid
r dimensionless radial coordinate
r_p particle radius
R gas constant
Re particle Reynolds number defined in Eq. (2–19)
ss dimensionless Southerland's constant defined in Eq. (2–24)
t dimensionless time
T dimensionless gas temperature
T_0 gas temperature at stagnation state
T_p dimensionless particle temperature
u dimensionless gas-phase axial velocity
u_p dimensionless particle-phase axial velocity
$\vec{u}_j$ vectors defined in Eq. (3–11) ($j=t, x, y$)
v dimensionless gas-phase radial velocity
v_p dimensionless particle-phase radial velocity
w dimensionless gas-phase circumferential velocity
w_p dimensionless particle-phase circumferential velocity
x dimensionless axial coordinate; horizontal coordinate
y vertical coordinate
α coefficient defined in Eq. (3–5)
β coefficient defined in Eq. (3–6)
γ gas specific heat ratio; coefficient defined in Eq. (3–7)
ε gas emissivity
ε_p particle emissivity
η transformed dimensionless radial coordinate
μ dimensionless gas viscosity
μ_0 gas viscosity at stagnation state
ξ transformed dimensionless axial coordinate
ρ dimensionless gas density
ρ_0 gas density at stagnation state
ρ_p dimensionless particle density
σ Stefan-Boltzmann constant

Superscripts

$\rightarrow$ vectored quantity

Subscripts

$_0$ reference state

$_p$ particle-phase

References

[1] I-Shih Chang, One- and Two-Phase Nozzle Flows, AIAA J. **18**, No. 12, 1980, pp. 1455–1461.

[2] J.F. Regan, H.D. Thompson and R.F. Hogland, Two-Dimensional Analysis of Transonic Gas-Particle Flows in Axisymmetric Nozzle, J. Spaceraft, Apr. 1971, pp. 346–351.

[3] R.F. Hoglund, Recent Advances in Gas-Particle Nozzle Flows, ARS J. May 1962, pp. 662–671.

[4] T. Doi, Gas-Particle Nozzle Flows and Optimum Nozzle Shap, ISAS Rep. No. 596, Nov. 1981.

[5] A.R. Gourlay and J. Ll. Morris, Hopscotch Difference Methods for Nonlinear Hyperbolic Systems, IBM J. Res.& Develop., **16**, No. 4, July 1972, pp. 349–353.

[6] A.R. Gourlay, A fast Second-Order Partial Differencial Equation Solver, J. Inst. Math. & Its Appl., **6**, No. 4, Dec 1970, pp. 375–390.

[7] D.J. Carlson and R.F. Hoglund, Particle Drag and Heat Transfer in Rocket Nozzles, AIAA J., **2**, No. 11, Nov. 1964, pp. 1980–1984.

[8] J.F. Thompson, F.C. Thames and C.W. Mastin, Boundary-Fitted Curvilinear Coordinate Systems for Solution of Partial Differential Equations on Fluid Containing any Number of Arbitrary Two-Dimensional Bodies, NASA CR-2729, 1977.

[9] R. W. MacCormack and B. S. Baldwin, A Numerical Method for Solving the Navier-Stockes Equations with Application to Shock-boundary Layer Interactions, AIAA Paper, Pasadena, Calif., Jan. 1975.

[10] R.F. Cuffel, L.H. Back and P.F. Massier, Transonic Flow Field in Supersonic Nozzle with Small Throat Radius of Curvature, AIAA J., **7**, No. 7, July 1969, pp. 1364–1366.

[11] R.A. Serra, Determination of Internal Gas Flows by a Transient Numerical Technique, AIAA J., **10**, No. 5, May 1972, pp. 603–611.